PNAS
www.pnas.org

Supplementary Information for

Integrins protect sensory neurons in models of paclitaxel-induced peripheral sensory neuropathy

Grace Ji-eun Shin[1*], Maria Elena Pero[2,3], Luke A. Hammond[1], Anita Burgos[1], Atul Kumar[2], Samantha E. Galindo[1], Tanguy Lucas[1], Francesca Bartolini[2] and Wesley B. Grueber[1,4,5]

[1]Columbia University, Zuckerman Mind Brain and Behavior Institute, Jerome L. Greene Science Center, 3227 Broadway, New York, NY, 10027 USA, [2]Columbia University, Pathology & Cell Biology, New York, NY, 10032 USA, [3]Department of Veterinary Medicine and Animal Production, University of Naples Federico II, 80137, Naples, Italy, [4]Columbia University, Physiology and Cellular Biophysics, New York, NY, 10032 USA, [5]Columbia University, Neuroscience, New York, NY, 10027 USA

* Correspondence to:

Grace Ji-eun Shin
Columbia University, Zuckerman Mind Brain and Behavior Institute, Jerome L. Greene Science Center, 3227 Broadway, L9-005, New York, NY, 10027 USA.
E-mail: js4920@columbia.edu

This PDF file includes:

Supplementary Information Materials and Methods
Figures S1 to S12
Table S2
SI References

Other supplementary materials for this manuscript include the following:

Table S1

Supplementary Information Materials and Methods

Fly stocks

UAS-αPS1 (*multiple edematous wings, mew*) on III and *UAS-βPS* (*myospheroid, mys*) on III were provided by Dr. K. Broadie (Vanderbilt University). *UAS-Ncad*$^{7b\text{-}13a\text{-}18b}$ (on II) line was provided by Dr. Chi-Hon Lee (National Institute of Health). *ppk1.9-Gal4* (II), *ppk-CD4-tdGFP* (III) and *ppk-CD4-tdTom* (III), and *412-Gal4* have been described previously (1-4). *w*^{1118} and *UAS-Rab4-mRFP, UAS-Spin-myc-mRFP, UAS-YFP-Rab4-WT, UAS-βPS-RNAi,* and *UAS-TrpA1* lines were obtained from the Bloomington Stock Center (Bloomington, IN). Full genotypes of the animals used in the study can be found in Table S2.

Larval assay setup for paclitaxel treatment

Paclitaxel (Tocris Bioscience) was diluted to 5 mM in ethanol, aliquoted and stored in -80 °C until use. Fresh aliquots of paclitaxel were diluted to a final concentration of 1, 10, 20, or 30 µM in 1X PBS. A matching concentration of ethanol was added as a vehicle control. This solution was used to make food using instant *Drosophila* medium (Formula 4-24 ®, Carolina Biological Supply Company) immediately before starting the larval assay. Embryos were collected on grape plates with yeast paste made with 0.5 % propionic acid. First instar larvae (24 – 28h AEL) were collected manually with a paint brush, washed in 1X PBS, and placed into paclitaxel-containing food. Larvae were reared at 25°C and were stage-matched to late third instar (based on the morphology of anterior spiracles) at the time of collection. Controls typically reached late third instar by 5-7 days. Any remaining animals that did not reach late third instar by 10 days after starting the treatment were discarded. All animals matching the developmental criteria were collected to avoid any selection bias. For acute treatment, second instar or early third instar larvae were collected manually (Fig. 5 *A*) directly from standard molasses *Drosophila* media, washed in 1X PBS, and placed into paclitaxel-containing food. Larvae were reared at room temperature for either 48 h or 72 h. Only larvae that reached late third instar were collected for subsequent live imaging.

Global activation heat nocifensive assay and behavioral analysis

Global activation heat nocifensive assays were performed as previously described (1). Briefly, a single late third instar larva (stage-matched) was placed on a 0.6 % black ink gel (Super Black India ink, Speedball) in 1 % agarose in ddH_2O heated to 40 ˚C by a Peltier device (CP-031, TE technology) equipped with a temperature controller (TC-36–25-RS232, TE technology). Animals with an identical set of transgenes compared to experimental groups, with the exception of UAS transgenes, were used as a genotype control. Where possible, paclitaxel-treated animals were set up 2-3 days prior to control, so that both control and paclitaxel-treated animals could be tested for nocifensive behavior on the same day. Behaviors were recorded for 30 or 60 seconds, and quantified blindly. The number of 360˚ rolls was scored by using trachea as a reference for the dorsal region of the larva.

Subcloning and lentiviral packaging of human ecto-tagged ITGB1

Ecto-tagged human β1 integrin (ecto-GFP-ITGB1) in lentiviral expression vector (5) was provided by David Calderwood's lab at Yale University. pLENTI CMV Puro DEST (Eric Campeau, plasmid #17452), mTagRFP-T-Rab4a-7 (Michael Davidson, plasmid #58025), and Lamp1-mRFP-FLAG (David Sabatini, #34611) were purchased from Addgene. mTagRFP-T-Rab4a-7 was subcloned into pLENTI CMV Puro DEST plasmid using sequence ligation independent cloning (SLIC) method (6). Briefly, mTagRFP-T-Rab4a-7 was amplified using SLIC primers: forward tctagtccagtgtggtggaattctgcagatGCCACCATGGTGTCTAAG and reverse gattgtcgagcggccgccactgtgctggatCTAACAACCACACTCCTG, denoting sequences in uppercase to recognize the insert and lowercase to recognize the plasmid. The insert was cloned into the EcoRV linearized pLENTI CMV Puro DEST plasmid at plasmid to insert ratio of 1:5. T4 DNA polymerase containing mixture was incubated at room temperature for 45 sec, followed by 10 min incubation on ice before transformation into XL10-Gold® Ultracompetent cells (Agilent). The resulting plasmid was purified using transfection-grade plasmid purification kit (Qiagen) and confirmed by sequencing. Lentivirus production containing pLENTI CMV-ecto-GFP-ITGB1, pLENTI CMV-mTagRFP-T-Rab4a-7, pLENTI CMV-Lamp1-mRFP-FLAG, and pLENTI CMV Puro DEST were optimized with reference to methods described in Gornstein and Schwarz (7). Lentiviral expression vectors and packaging vectors (pLP1, pLP2, and pLP/VSVG, Thermofisher) were co-transfected to HEK293T cells using the calcium phosphate transfection method (8). Media containing viral particles

was collected 24, 36, 48h after transfection, and lentiviral particles were filtered through 0.45 μm, and then concentrated by centrifuging at 25,900 RPM at 4 °C for 120 min (SW 32 Ti rotor, Beckman Coulter Optima Ultracentrifuge). The virus pellet was resuspended in Neurobasal media (Invitrogen), without any supplement, to concentrate 250-fold from the packaging cell media, and stored in 30 μL aliquots at -80 °C until use. 5 μL of lentivirus was added to 1 mL culture at days *in vitro* (DIV) 5, and ~30 % of the media was changed before paclitaxel administration at DIV 12. Expression of ITGB1 was checked by western blot and expression of Rab4 and Lamp1 was checked by red fluorescence upon transduction to DRG neurons.

Adult mouse DRG culture and paclitaxel treatment

All protocols and procedures used in this study to prepare primary culture of DRG neurons were approved by the Institutional Animal Care and Use Committee at Columbia University and according to Guide for the Care and Use of Laboratory Animals distributed by the National Institutes of Health. Dorsal root ganglia from 8- to 12-week-old C57Bl/6J mice of both sexes were dissected, dissociated and plated in a 12-well plate. Specifically, the spinal column was isolated immediately from a sacrificed mouse, and cut into approximately four pieces, including at the midline, to expose DRG for isolation. Each piece was dissected within 5 min, and the remaining tissue was placed on ice. Dissected DRG from cervical, thoracic and lumbar anatomical regions were immediately placed in HBSS (Life Technologies) or DMEM (Life Technologies) on ice. Once DRG were collected, visible traces of axon tracts were cleaned before incubating in 1 mg/mL collagenase A (Sigma) for 1 h at 37 °C. Following incubation, DRG were washed twice in DMEM followed by 0.05% trypsin (Life Technologies) in DMEM digestion for 2 min at 37 °C. After the digestion, cells were washed twice with Neurobasal medium supplemented with 2% B-27 (Invitrogen), 0.5 mM glutamine (Invitrogen), 10% FBS (Sigma) and 100 U/mL penicillin-streptomycin. DRG neurons were then dissociated by repeated gentle pipetting until no clumps were visible. Once dissociation was complete, cells were resuspended in supplemented Neurobasal media with 10% FBS to 1.8 mL (150 μL × 12 wells) and plated onto 12-well plates (over 18 mm coverslips) that had been coated overnight with 100 μg/mL poly-D-lysine (Sigma) at 37 °C and 10 μg/mL laminin (Life Technologies) for 1 h at 37 °C. After 30 min, 850 μL of supplemented Neurobasal media was added to each well without disturbing plated cells. At 4 DIV,

~30% of the media was changed and 10 μM AraC (Sigma) was administered to suppress growth of non-neuronal cells in culture. Approximately 30% of the media was again changed at 12 DIV prior to paclitaxel treatment. 1 μL of 1000X paclitaxel (stock concentration 50 μM) was added to each well containing 1 mL of media to achieve a final concentration of 50 nM. 1 μL of DMSO was added as a vehicle control.

Surface biotinylation assay

Surface biotinylation assays were performed three times using independent neuron preparations and analyzed by SDS-PAGE and western blotting as previously described (9, 10). Biotinylated surface and total ITGB1 were detected by using rabbit ITGB1 antibody (1:1000, Invitrogen, Catalog # PA5-29606) and the secondary anti-rabbit IgG monoclonal antibody coupled to infra-red fluorophore (Fluorescent TrueBlot® Anti-Rabbit IgG DyLight TM 800, 1:10000, Rockland Immunochemical). As a loading control for measuring total ITGB1 levels, GAPDH (mouse, 1:5000, Sigma Aldrich) was used. Images of the blots were acquired to capture all bands at a linear range using an Odyssey imaging system (LI-COR Biosciences) and the fluorescent intensity of the bands was quantified using Image Studio Lite v5.2 (LI-COR Bioscience). Total level of ITGB1 was normalized against GAPDH levels, and expression levels of ITGB1 after paclitaxel treatment was calculated as a % of ITGB1 expression levels after vehicle treatment for both total and surface protein fractions.

Immunolabeling

Immunolabeling of *Drosophila* larvae was performed largely as described previously (11). Briefly, late third instar larvae were dissected in 1X PBS, fixed in 4% paraformaldehyde (PFA, Electron Microscopy Sciences) in 1X PBS for 15 min, rinsed three times in 1X PBS + 0.3% Triton X-100 (PBS-TX), and blocked for 1 h at room temperature (RT) or overnight at 4 °C in 5% normal donkey serum (NDS) in PBS-TX (Jackson Immunoresearch). Primary antibodies were chicken anti-GFP (1:1000; Abcam), rabbit anti-DsRed (1:250, Clontech), and mouse anti-mys (1:10, CF.6G11, Developmental Studies Hybridoma Bank), diluted in 5% NDS in PBS-TX. Tissue was incubated overnight in primary antibodies at 4 °C and then washed in PBS-TX for 3 × 15 min at RT. Species-specific, fluorophore-conjugated secondary antibodies (Jackson ImmunoResearch) were used at 1:1000 in 5% NDS in PBS-TX,

and incubated overnight 4 °C. Tissue was rinsed in PBS-TX for 3 × 15 min with a final rinse in PBS. Tissue was mounted on poly-L-lysine coated coverslips, dehydrated 5 minutes each in an ascending ethanol series (30, 50, 70, 95, 2 × 100%), cleared in xylenes (2 × 10 min), and mounted in DPX (Fluka).

For immunolabeling of DRG neurons, cultures were fixed in 4% PFA in PBS for 10 min, permeabilized with 0.1% Triton-X in 1X PBS for 10 min, and blocked in 10% normal goat serum in PBS (NGS-PBS) for 1 h. NF200 (1:300, Aves Labs Catalog # NFH) was diluted in NGS-PBS and incubated overnight at 4 °C. Nuclei were stained with Hoeschst 33342 (1:1000, Sigma), which was incubated with NF200. Species-specific, fluorophore-conjugated secondary antibodies (Invitrogen) were used at 1:500 in 10% NGS-PBS and incubated for 2 h at the room temperature. Immunolabelled cells were then washed in 1X PBS and mounted in Fluoromount-G (Southern Biotech).

Image acquisition

Drosophila sensory neurons were imaged on a Nikon A1R laser scanning confocal microscope using a 20x 0.75 NA Plan Apochromat objective and a Yokogawa W1 spinning disk confocal microscope mounted on a Nikon Ti2-E stand using a 20x 0.75 NA Plan Apochromat objective. To avoid any selection bias, all animals from each experiment were imaged, and up to four ddaC nociceptive neurons were selected from abdominal segments. These cells were sequentially imaged in z-stacks from anterior to posterior positions in each larva. One cell per larva was selected for quantification blind to the genotype and the treatment according to following rules. The first cell was selected from each animal if this cell was not damaged during dissection or severely distorted from mounting (i.e., dendrites did not cross due to folding). If the first cell was damaged or distorted, the next intact cell was selected in the order of image acquisition. If all cells were damaged or distorted in a given animal, then the animal was not analyzed. A Yokogawa W1 spinning disk confocal microscope mounted on a Nikon Ti2-E stand using a 20x 0.75 NA Plan Apochromat objective was used to image mouse DRG neurons. Images were collected initially in a 6 mm × 6 mm square in 2D, avoiding the peripheral region of the cultured cells. Three random points were selected from this image, which served as the center of non-overlapping z-stack images of 2 × 2 mm^2 each.

Image analysis

Prior to tracing of nociceptive neurons, an image containing a single neuron was blinded and the background was cleaned using background subtraction and non-local means denoising in Fiji (12). Axons were manually removed together with any neuronal arbors from neurons in adjacent segments. To improve automatic detection of arbors, brightness and contrast were optimized before processing in Vaa3D. The Vaa3D neuron 2 auto tracing plugin (13) was used to generate tracings of neuronal arbors. Any errors found in an automatically traced file were manually corrected via manual annotation using editing tools included in the neuron 2 plugin. The global neuron feature option was used to extract quantitative information from the reconstruction.

All data collected from *Drosophila* were randomized and blinded prior to quantification using customized Python codes. Sites of degeneration and crossing were scored using the Fiji multi-point tool (12). We counted varicosities and fragmentation as early and late signs of degeneration, respectively. For quantifying branch crossing, we scored terminal dendrite crossing when at least one arbor was terminal neurite. All imaging data collected from DRG axons was blinded prior to quantification. For quantifying DRG degeneration phenotypes, a degeneration index was calculated as described in Gerdts et al., 2011 (14). Quantification was performed blindly using Fiji by an independent researcher who was not involved in experimentation and imaging. Briefly, images were automatically thresholded (global threshold) using a default auto-threshold method, binarized, and then total and fragmented axon areas were measured by using the particle analyzer plugin of Fiji. The default automatic threshold in Fiji was calculated by first dividing the image into objects and background using a test threshold, followed by computing the threshold that is equal or smaller than the composite average determined as (average background + average objects)/2. A circularity, determined as (area) / ($\pi \times \text{radius}^2$) and was calculated for each particle. Any particle of higher than 0.2 for circularity was considered fragmented. The degeneration index was calculated as a ratio of fragmented axon area over total axon area (14).

The local density of *Drosophila* sensory arbors was measured using a two-step custom Fiji macro. All images used for local density analysis were collected using identical settings on a Nikon A1R scanning laser confocal microscope. Prior to

performing the density analysis, the image files containing a single neuron were subjected to background subtraction and non-local means denoising, and then automatically thresholded and binarized. Axons were manually removed together with any neuronal arbors from neurons in adjacent segments. Using a custom Fiji script, local density was measured by a repeated measurement (sampled every 8 px in a 2048 × 2048 px image) of % of area occupied by the branches within a 50 × 50 μm^2 square area, ignoring soma. Using these values, a heatmap was generated that shows absolute levels of density (up to 15%) in assigned colors so that different images can be directly compared for their density levels and distribution. To generate local density relative to distance from the soma, the values from the heatmap were binned according to the distance from soma and mean and standard deviation was calculated for each neuron. To calculate the distribution of density values across the entire neuron, a custom Python script was used to measure the area of receptive field of each neuron, and the number of pixels in a given density (0-20%) in each neuron. All scripts used for density analysis are available on Github (https://github.com/lahammond/Neuron_Density_Analysis).

Live imaging and quantitation of Rab4 and lysosomes in *Drosophila* larvae

We prepared larvae for live imaging according to a previously described method (15). Briefly, a drop of fresh 3% agarose in ddH_2O was placed on a slide and dried overnight at 65°C before use. Single larvae were cleaned, placed on the dried agarose patch, and gently squeezed by a coverslip (size #1, Thorlab). This sandwich was held in place with sticky tape. Once mounted, the larva was imaged within 45 min. For chronic paclitaxel treatment, live imaging was performed using Nikon A1R point-scanning laser confocal microscope (x40 objective, oil, 1.3 NA, 200 µm WD, CFI60 Plan Fluor). Nociceptive neurons were identified by their expression of *ppk-CD4-tdGFP* and a single image was collected as a reference map for the selection of ROIs. ROIs (256 x 128 px) were selected to image ~50 µm of primary dendrite at a Nyquist resolution. For both Rab4 and Spinster, we chose ROIs at primary branches sufficiently away from soma, typically at around the first branch point (>100 µm from soma). A single section of this ROI was imaged at 1.1 sec/frame. For acute paclitaxel treatment (48 and 72 h), live imaging was performed using a Yokogawa W1 spinning disk confocal microscope mounted on a Nikon Ti2-E stand (40x objective, water, 1.15

NA, CFI60 Plan Fluor). Nociceptive neurons were identified by the presence of either Rab4-RFP or Spin-RFP blind to the morphology of neuronal arbors. ROIs (243 x 243 μm^2) that include cell body within second and third quarters of the area was selected to image all visible dendrites. A single section of this ROI was imaged at 1 sec (Rab4) or 2 sec (Spin)/frame. After the completion of live imaging, a z-series of the nociceptive neuron and Rab4/Spin in the same ROI was collected for quantification of degeneration and branch crossings. For both imaging conditions, focus was manually adjusted when necessary to counter minor movements of the animal. Images were collected for up to 5 minutes depending on the stability of the mounted larva. All images were randomized and blinded before any correction or quantification. Images were corrected for minor movements using the Stackreg plugin for Fiji. For quantification of Rab4 for chronic treatment, we used the Kymoanalyzer v.1 plugin for Fiji (16) with default settings, except the threshold range for static vesicles was adjusted to avoid false positive detection of trafficking due to the movement of animal. Upon quantification, we plotted values including net vesicle population distribution (stationary, anterograde, and retrograde), net velocity of vesicles in anterograde and retrograde directions, switch frequency, and track density. For quantifying Rab4 after acute treatment, a single 30-second block from each kymograph was selected for quantifying the number of total, mobile, and stationary vesicles in Fiji. Total number of vesicles was estimated by counting the number of peaks in a distribution curve generated by the line plot tool across the x axis of the kymograph at 10 px. Mobile vesicles were manually counted using the multi-point tool, which was then used to calculate the number of stationary vesicles. Total number of vesicles were normalized by the length of the dendrite selected in the ROI. For quantification of Spin vesicles, a 20-sec (chronic) or a 40-sec (acute) portion of each kymograph was selected blindly to include the portion of kymographs with minimal animal movement. The fluorescent intensity of this portion, representing the average area occupied by lysosomes in the dendrite, was measured in Fiji using the line plot tool. Due to the frequent movement of larvae in the z-axis during imaging, we found that vesicles were often out-of-focus, potentially affecting our intensity-based quantification. We found that average fluorescence intensity levels above 3000 a.u. represent an immobile Spin positive signal in a given location in all of our recordings. Therefore, we determined 3000 a.u. as a maximum value for average fluorescence

intensity levels. Average fluorescent intensity values were plotted as a distribution curve and area under the curve was calculated and normalized by the length of the dendrite selected in the ROI.

Superresolution imaging and quantification of integrins and Rab4

Images were collected by using a vt-iSIM (VisiTech International) (17) mounted on a Leica Dmi8 microscope using a 93x 1.3 NA HC PL APO glycerol objective and a Yokogawa CSU-W1 SoRa mounted on a Zeiss Axio Observer using a 100x 1.46 NA Alpha Plan-Apochromat oil objective. Acquisitions included the cell body, axon and dendrites of ddaC neurons. These images were subsequently deconvolved using Microvolution (20 iterations), and were blinded prior to analysis. An Ilastik (18) project, pretrained on these datasets, was used to perform pixel classification, with the resulting probability images used for segmentation and object analysis in Imaris (Oxford Instruments). Briefly, nociceptive neurons (ppk-CD4-tdTom) were segmented (smoothing 0.130 μm and an absolute threshold set to an intensity representing greater than 30% probability) to isolate internal integrin and Rab4 expression. Channels for integrin βPS (anti-βPS) and Rab4-YFP, respectively, were segmented using 0.065μm smoothing, and an absolute threshold set to an intensity representing greater than 50%. To separate touching objects a split setting (0.5μm) was used, with resulting objects filtered to exclude those with fewer than 15 voxels. Detected objects were compartmentalized into their locations in soma, dendrite, and axon via manual annotation of neuronal surfaces. Co-localization of object expressing both βPS and Rab4 were detected by categorizing Rab4 positive objects as single (Rab4 alone) or co-positive (Rab4 and integrins).

Imaging and quantitation of Rab4 and lysosomes in mouse DRG neurons *in vitro*

DRG neurons from adult mice were prepared as described in the materials and methods in the main text. The dissociated adult DRG neurons cultured in 35mm glass bottom dish (MatTek) was transduced at 12 h after plating with mTagRFP-T-Rab4a-7 (Rab4) or Lamp1-mRFP-FLAG (Lamp1) packaged in lentivirus. At 12 DIV, 1 μL of 1000X paclitaxel (stock concentration 50 μM) was added to each well containing 1mL of media to achieve a final concentration of 50 nM. 1 μL of DMSO was added as a vehicle control. Images were acquired using a 60x 1.49 NA Apochromat TIRF oil

objective on Nikon Ti T3 microscope (Nikon Ti) coupled to Andor iXon X3 camera and equipped with a temperature controlled (37 °C) CO_2 incubator. Specifically, proximal regions from intact axons (within 100 μm from the cell body) were selected for imaging and movies were acquired at 2 s/frame for 5 min at 0, 24, 48 h after the paclitaxel treatment. Kymographs were generated manually in Fiji by tracing the proximal axon using a segmented line tool. Dynamic states of Lamp1 positive and Rab4 positive vesicles were identified on kymographs and classified as stationary or mobile. For mobile vesicles, they were further categorized as "jittery" (travel length < 5 pixels) or "running" regardless of the direction. Using the comparable condition, dissociated adult DRG neurons cultured in glass bottom dish treated with either paclitaxel or DMSO were fixed and immunolabelled with chicken NF200 and followed by species-specific and fluorophore-conjugated secondary antibodies. Prepared samples were used for batch control and degeneration analysis. Images of less than 10 random fields of view (440 x 328 μm^2) were collected per treatment condition using a 20x 0.45 NA LUCPlan FLN objective on Olympus IX81 inverted fluorescence microscope coupled to a Sensicam QE cooled digital 12-bit CCD camera (Sensicam QE; Cooke Corporation). Degeneration index was calculated as described in Image Analysis section.

Statistical analysis

Prism 8 was used for all statistical analysis and plotting data. Gaussian distribution was determined by using Kolmogorov-Smirnov or Shapiro-Wilk normality test for all experiments, except the surface biotinylation assay. Depending on this test, either parametric or non-parametric tests were selected for each analysis. For comparing three or more groups, a post-test was performed to correct for a multiple comparison to obtain an adjusted p-value. Except branch density analyses and Sholl analysis, all other data were subjected to a homoscedasticity test; F-test, Brown-Forsythe test, or Spearman's rank correlation test was employed depending on the number of the groups and factors within the dataset. The data with heteroscedasticity were subject to Welch's t-test, Brown-Forsythe and Welch's ANOVA, or Kolmogorov-Smirnov test. For repeated measures tests to test null hypotheses in branch density analyses and Sholl analysis, a mixed effect model using restricted maximum likelihood (REML) was used without assuming sphericity in the dataset and corrected for violating sphericity using Geisser-Greenhouse's epsilon. Detailed description of all statistical

results for each experiment is included in figure legends and Table S1. P values (two-tailed) were noted in graphs or in Table S1.

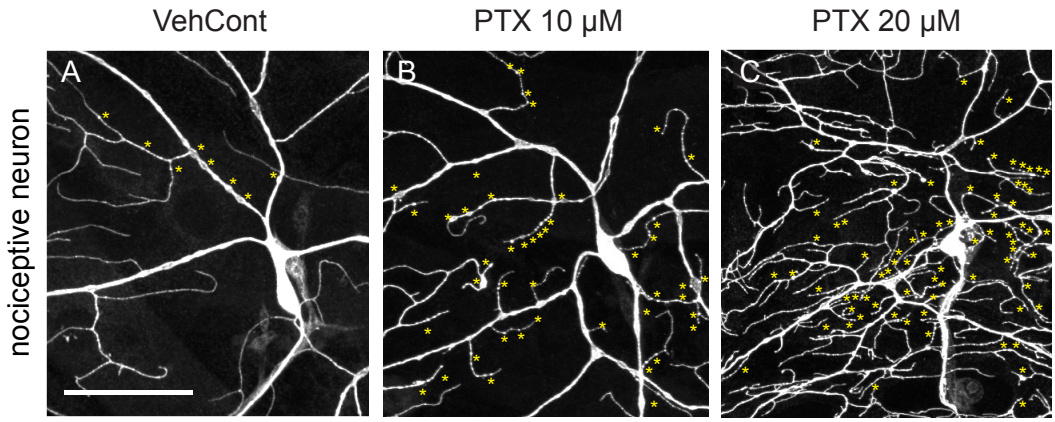

Fig. S1. Degeneration phenotypes in neurons presented in Figure 1

Enlarged views of cell body and proximal arbors of neurons from Fig. 1 *A–C* to show varicosities and fragmentation (yellow asterisks). See also Fig. 2.

Scale bars = 50 µm

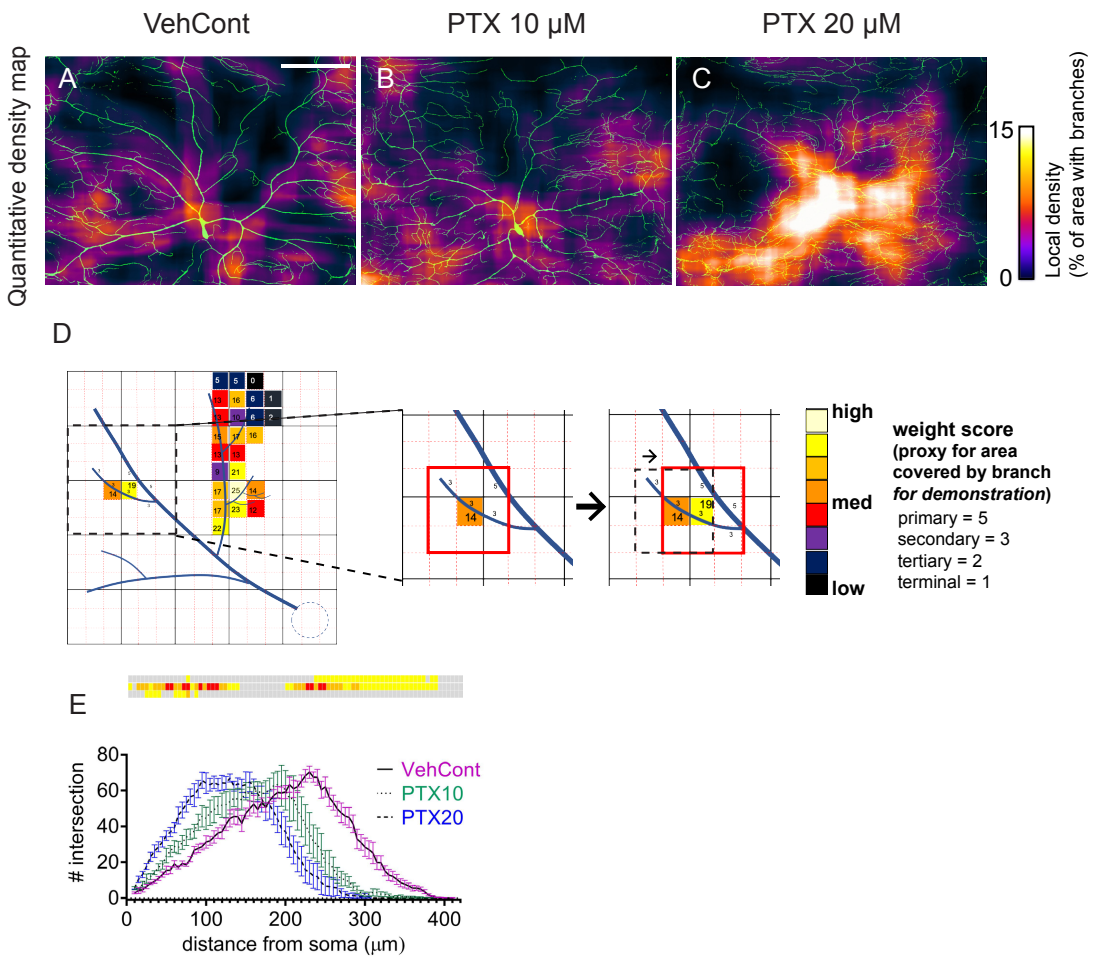

Fig. S2. Generation of density maps for quantification of sensory arbors

(*A–C*) Quantitative density heatmaps of arbors shown in Fig. 1. Density (% area covered by branches) was measured every 2.5 µm (8 px in 2048 x 2048 px image). This process results in 65536 coded squares, or measurement points (256 x 256) per image obtained in our study. Most of the density values were lower than 15 %, therefore we assigned the color for each measurement point corresponding to the scale of 0-15 % to create the heatmap.

(*D*) Simplified illustration of density analysis. We used the weight score as a proxy for % of area covered by branches in this illustration. Dotted red boxes indicate each measurement point (15 x 15 measurement points tiling the arbor field in the first schematic), the solid red boxes indicate the area surrounding each tile (3 x 3 boxes) that demarcates the area that is used to calculate the value of the measurement point in the center. Each color-coded measurement point therefore shows the density of the 3 x 3 surrounding area, calculated according to the weight score for primary, secondary, etc. branches. The color is assigned according to the scale (high-med-low).

Simulation of the density measurement of two measurement points is illustrated in the two enlarged schematics. The weight score of the 3 x 3 red box for the first and the second measurement points have density scores of 14 and 19. They are mid and mid-high densities for this schematic neuron, therefore had been assigned dark orange and yellow colors in the map. The red box scans along the entire image to calculate the density for each center point, creating the arbor heatmap.

(*E*) Sholl analysis of the same set of neurons used in density analysis (Fig. 1 *D* and *E*). The Sholl Analysis Fiji plugin was used at an interval of 5 μm, starting from 10 μm away from soma (19).

Scale bar=100 μm. Error bars denote standard error means. Mixed effect analysis with Tukey's multiple comparison post-test (See also Table S1). Statistical results from E are shown in color-coded boxes. Top row: Veh Cont *vs.* PTX10; middle row: Veh Cont *vs.* PTX20; bottom row: PTX10 *vs.* PTX20. $p<0.05$ (yellow), $p<0.01$ (orange), $p<0.001$ (red), $p>0.05$ (gray).

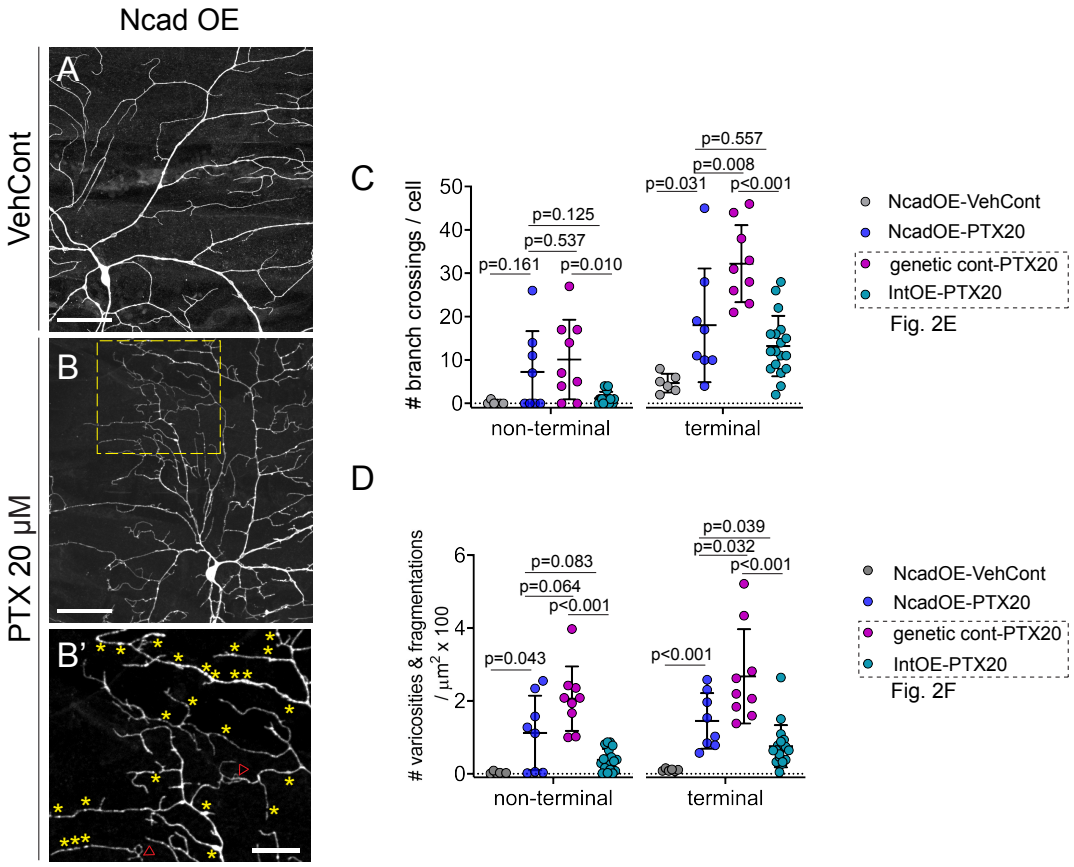

Fig. S3. N-cadherin overexpression in nociceptive neurons is partially protective against paclitaxel-induced morphological phenotypes.

(*A–B'*) Confocal micrographs of nociceptive neurons from N-cadherin overexpressing animals harboring *ppk1.9Gal4, ppkcd4tdgfp,* and *UAS-Ncad*$^{7b\text{-}13a\text{-}18b}$ treated with vehicle control (VehCont) and paclitaxel (PTX 20 µM). (*B'*) Enlarged image of area in *B* (dashed yellow box) showing varicosities (yellow asterisks) and crossings (red arrow heads).

(*C* and *D*) Quantification of paclitaxel-induced phenotypes, degeneration and branch crossings in non-terminal and terminal dendrites in N-cadherin overexpressing animals compared to paclitaxel-treated genetic control and integrin overexpressing animals from Fig. 2. Each data point represents a single cell from one larva. Data were collected from two (NcadOE-VehCont) and three (NcadOE-PTX) independent experiments, respectively.

Scale bars=50 µm (*A* and *B*) and 20 µm (*B'*). All error bars denote standard deviation. Kolmogorov-Smirnov test or Welch's t-test (*C*, non-terminal; *D*), one-way ANOVA with Tukey's multiple comparison post-test (*C*, terminal). See also Table S1 for further statistical results.

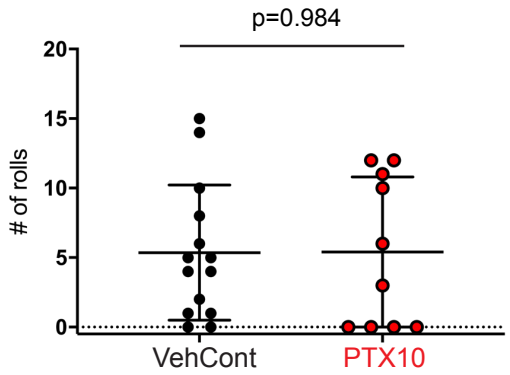

Fig. S4. Nocifensive responses arising from thermogenetic activation of DnB interneurons are not sensitive to paclitaxel treatment.

Larvae expressing *UAS-TrpA* under the control of *412-Gal4* were reared to wandering third instar stage. Animals were tested for rolling behavior induced by global thermal stimuli (Peltier device at 31°C). Data were collected from three independent experiments. Quantification of rolling behavior was performed by counting the number of rolls within 30 seconds upon thermal stimuli to the larva. Unpaired t-test. Error bars = S.D.

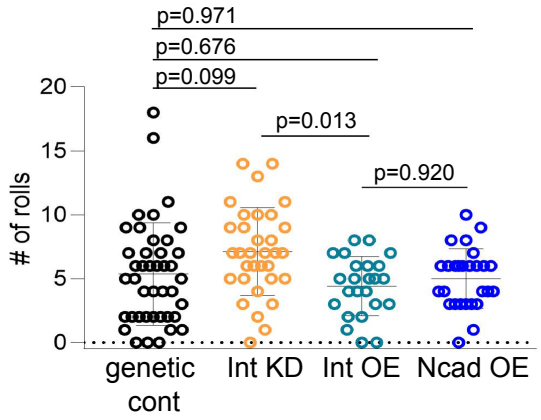

Fig. S5. Nocifensive responses in *Drosophila* larvae with changes in integrin levels or N-cadherin overexpression.

Larvae of matching genotype to morphological analysis in Fig. 2 and Fig. S3 were used to test baseline nocifensive behavior. All animals harbor *ppk1.9Gal4, ppkcd4tdgfp.* Genetic cont (lacking *UAS*), Int KD (*UAS βPS RNAi*), Int OE (*UAS-αPS1*, *UAS-βPS*), Ncad OE (*UAS-Ncad*$^{7b\text{-}13a\text{-}18b}$). Animals were reared to late third instar stage and tested for nocifensive responses to global thermal noxious stimuli (Peltier device at 41°C). Data were collected from four independent experiments. Quantification of rolling behavior was performed by counting the number of rolls within 60 seconds upon thermal stimulation of the larva. One-way ANOVA with Tukey's multiple comparison post-test. Error bars = S.D. See also Table S1 for further statistical results.

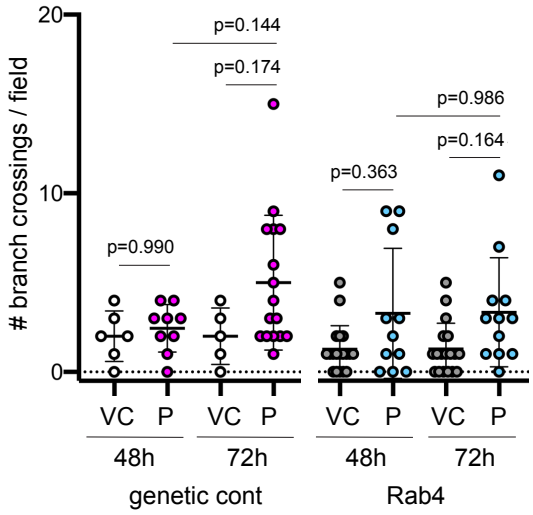

Fig. S6. Effect of 48 and 72 h paclitaxel administration on branch crossings in *Drosophila* nociceptive neurons

Neither wild type nor Rab4 expressing nociceptive neurons showed significant changes in branch pattern, scored by the number of branch crossings after 48 h and 72 h of paclitaxel administration at 20 μM. By 72 h, both genotypes treated with paclitaxel showed a modest increase in the number of branch crossings. VC: vehicle control, P: 20 μM paclitaxel. Data were collected from genetic cont-VC 48 h $N = 2$ (4 animals), genetic cont-VC 72 h $N = 2$ (3 animals), genetic cont-P 48 h $N = 2$ (4 animals), genetic cont-P 72 h $N = 2$ (5 animals), Rab4-VC 48 h $N = 4$ (10 animals), Rab4-VC 72 h $N = 2$ (7 animals), Rab4-P 48 h $N = 2$ (5 animals), Rab4-P 72 h $N = 2$ (4 animals). Each data point represents a quantification from a single cell, n=1-3 cells collected from each animal. One-way ANOVA with Tukey's multiple comparison post-test (genetic cont) and Kolmogorov-Smirnov test (Rab4). Error bars = S.D. Field size is 243 x 243 μm^2, a full field of view using a x40 objective including the center of a single cell. See also Table S1 for further statistical results.

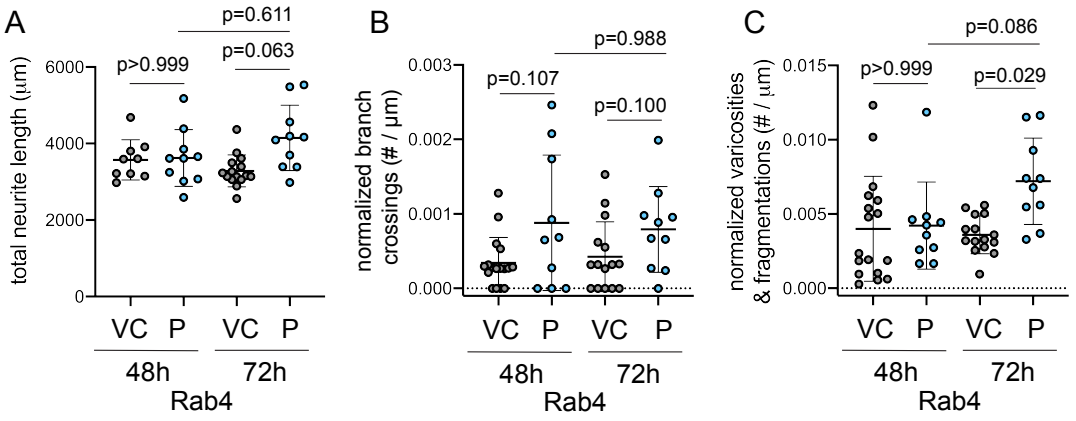

Fig. S7. Normalized effects of 48 and 72 h paclitaxel administration on Rab4-expressing *Drosophila* nociceptive neurons.

(*A*) Total neurite length was measured from axon and dendrites in the field defined in Fig. S6.

(*B* and *C*) Numbers of branch crossings (*B*) and varicosities and fragmentation (degeneration phenotypes) (*C*) were normalized to total neurite length. Statistical analyses indicate that 72 h, but not 48 h, treatment of paclitaxel-induced degeneration of nociceptive arbors. Each data point represents a quantification from a single cell, n=1-3 cells collected from each animal. VC: vehicle control, P: 20 µM paclitaxel. Data were collected from Rab4-expressing neurons in larvae fed vehicle (VC) 48 h N=4 (10 animals), Rab4-VC 72 h N=2 (7 animals), paclitaxel (P) 48 h N=2 (5 animals), or Rab4-P 72 h N=2 (4 animals). Brown-Forsythe and Welch's ANOVA with Dunnett's T3 multiple comparison post-test (*A*), Kolmogorov-Smirnov test (*B*), Kruskal-Wallis test with Dunn's multiple comparison post-test (*C*). Error bars = S.D. See also Table S1 for further statistical description.

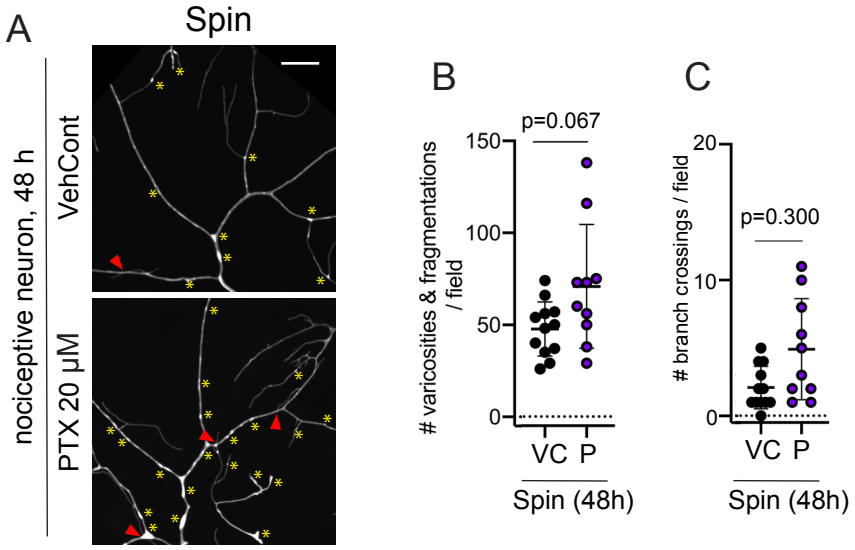

Fig. S8. Effects of 48 h paclitaxel administration on Spin-expressing *Drosophila* nociceptive neurons

Examples of confocal micrographs (*A*) and quantification of the integrity of nociceptive dendrites after paclitaxel treatments for 48 h in Spinster expressing nociceptive neurons. Degeneration (*B*) and branch crossings (*C*) were quantified using images collected from live animals. Animals harbor a nociceptive neuron driver and a marker (*ppk1.9Gal4, ppkcd4tdgfp*) with *UAS-Spin-myc-mRFP* (Spin). Yellow asterisks indicate varicosities and fragmentation and red arrowheads indicate crossing branches. Data were collected from Spin-expressing neurons in larvae fed vehicle (VehCont, VC) for 48 h $N = 2$ (5 animals) or paclitaxel (PTX20, P) for 48 h $N = 2$ (5 animals). Each data point represents a quantification from a single cell, n=1-4 cells collected from each animal. Error bars = S.D. Field size is 243 x 243 µm^2, a full field of view using a x40 objective including the center of a single cell. Scale bar= 20 µm, applies to both panels. Welch's t-test (*B*) and Kolmogorov-Smirnov test (*C*).

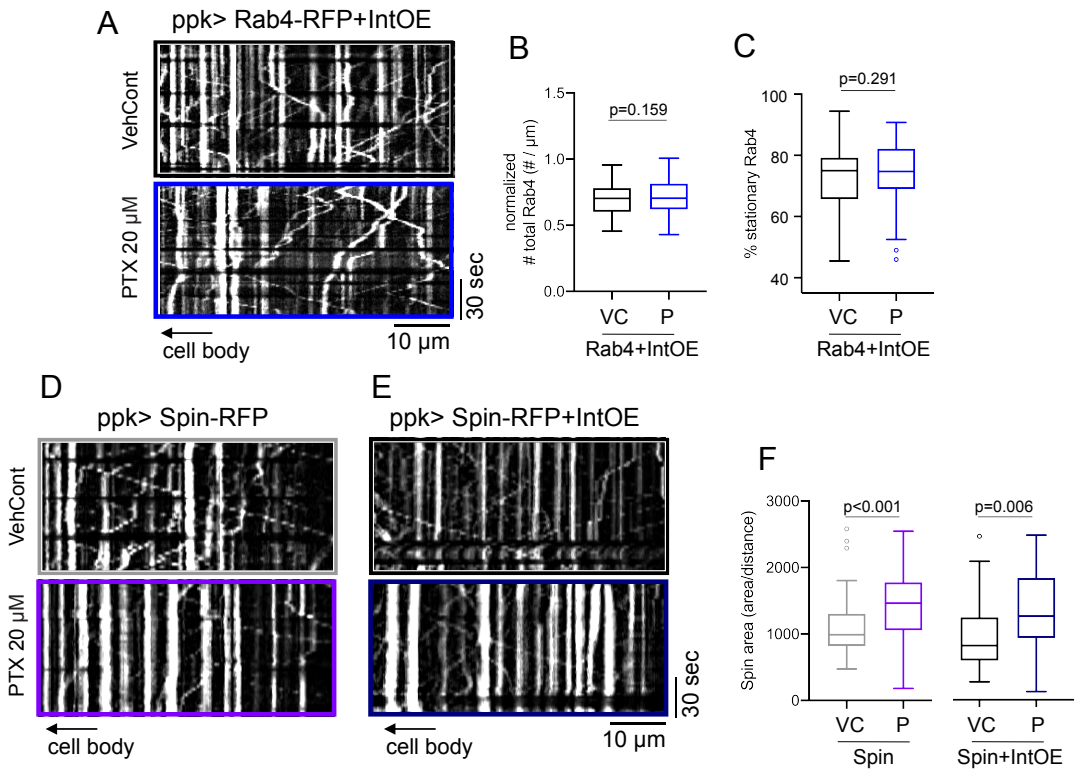

Fig. S9. Integrin overexpression prevents paclitaxel-induced changes in Rab4-positive vesicles

(*A–C*) Rab4-mRFP was expressed in nociceptive neurons along with integrins (*UASαPS1, UASβPS*) using *ppk1.9-Gal4, ppkcd4tdgfp*.

(*B* and *C*) Quantification of Rab4 vesicles. Numbers of total Rab4 and the proportion of stationary Rab4 do not differ between vehicle control (VC) and paclitaxel (P, at 20 µM) fed larvae. Data were collected from Rab4-IntOE VC 48 h $N = 3$ (9 animals) and Rab4-IntOE P 48 h $N = 3$ (7 animals). Number of individual kymographs used: Rab4+IntOE VC $n = 54$ and Rab4+IntOE P $n = 77$. 1-4 cells were selected from each animal and 1-4 kymographs were generated from each cell.

(*D* and *E*) Spin-myc-mRFP was expressed in nociceptive neurons of genetic control (*D*) or integrin overexpression (*E*, *UASαPS1, UASβPS*) background using *ppk1.9-Gal4, ppkcd4tdgfp* and the area occupied by Spin-positive vesicles was measured (*F*). Spin-positive area showed an increase in paclitaxel treated cells in both genetic control and integrin co-overexpression background. Data were collected from Spin VC 48 h $N = 2$ (5 animals), Spin P 48 h $N = 2$ (5 animals), Spin+IntOE VC 48 h $N = 3$ (7 animals), and Spin+IntOE P 48 h $N = 4$ (9 animals). Number of individual kymographs used: Spin control $n = 46$, Spin P $n = 59$, Spin+IntOE VC $n = 31$,

Spin+IntOE P n = 40. 1-4 cells were selected from each animal and 1-4 kymographs were generated from each cell.

(*A, D,* and *E*) Movements are visualized by kymographs in animals treated with vehicle and paclitaxel. All animals were treated with paclitaxel or vehicle for 48h starting from the early 3rd instar stage. Time and distance scale bars on E also apply to *D.* (*B, C,* and *F*) All data were plotted using Tukey's box and whiskers. Unpaired t-test (*B* and *C*) and Mann-Whitney test (*F*).

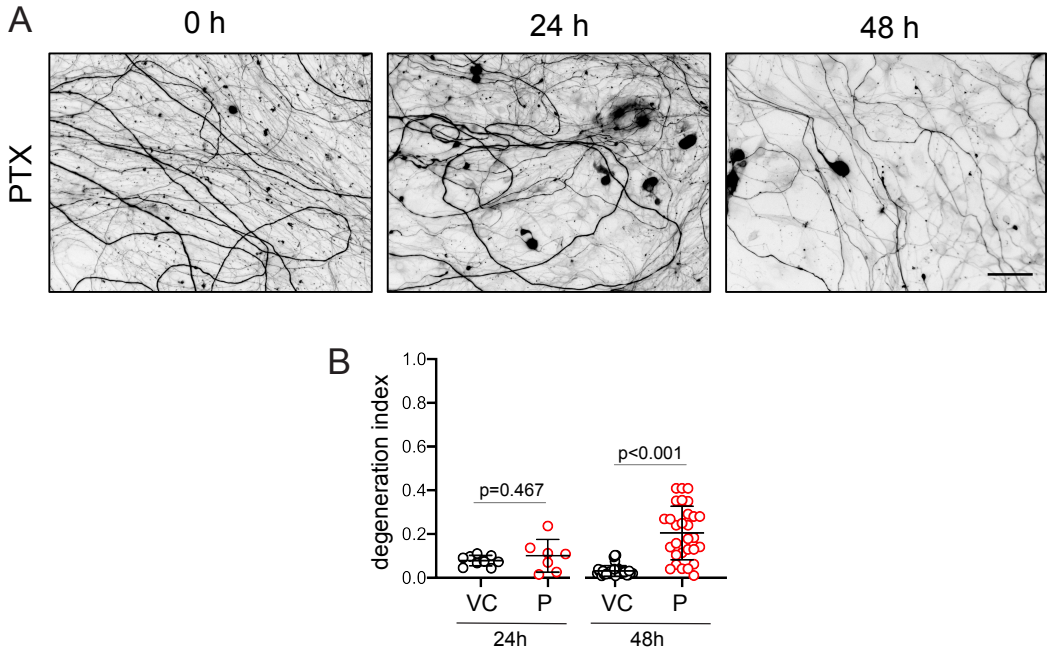

Fig. S10. Timeline for paclitaxel-induced degeneration in mouse DRG neurons.
(*A*) Images showing adult DRG neurons treated the same as cells prepared for live imaging experiments (Fig. S11), except for virus transduction. DRG neurons were treated with 50 nM of paclitaxel from DIV 12 and fixed immediately (0 h) or after 24 or 48 h incubation. Fixed cells were stained with NF200.
(*B*) Degeneration masks were generated, and the index was calculated as explained in Fig. S12. Paclitaxel treated cells showed a significant increase in degeneration at 48 h. Each data point refers to an independent field of view collected from two independent experiments. VC: vehicle control, P: 50 nM paclitaxel. Error bars = S.D. Scale bar = 50 µm, applies to all panels. Welch's t-test (24 h) and Kolmogorov-Smirnov test (48 h).

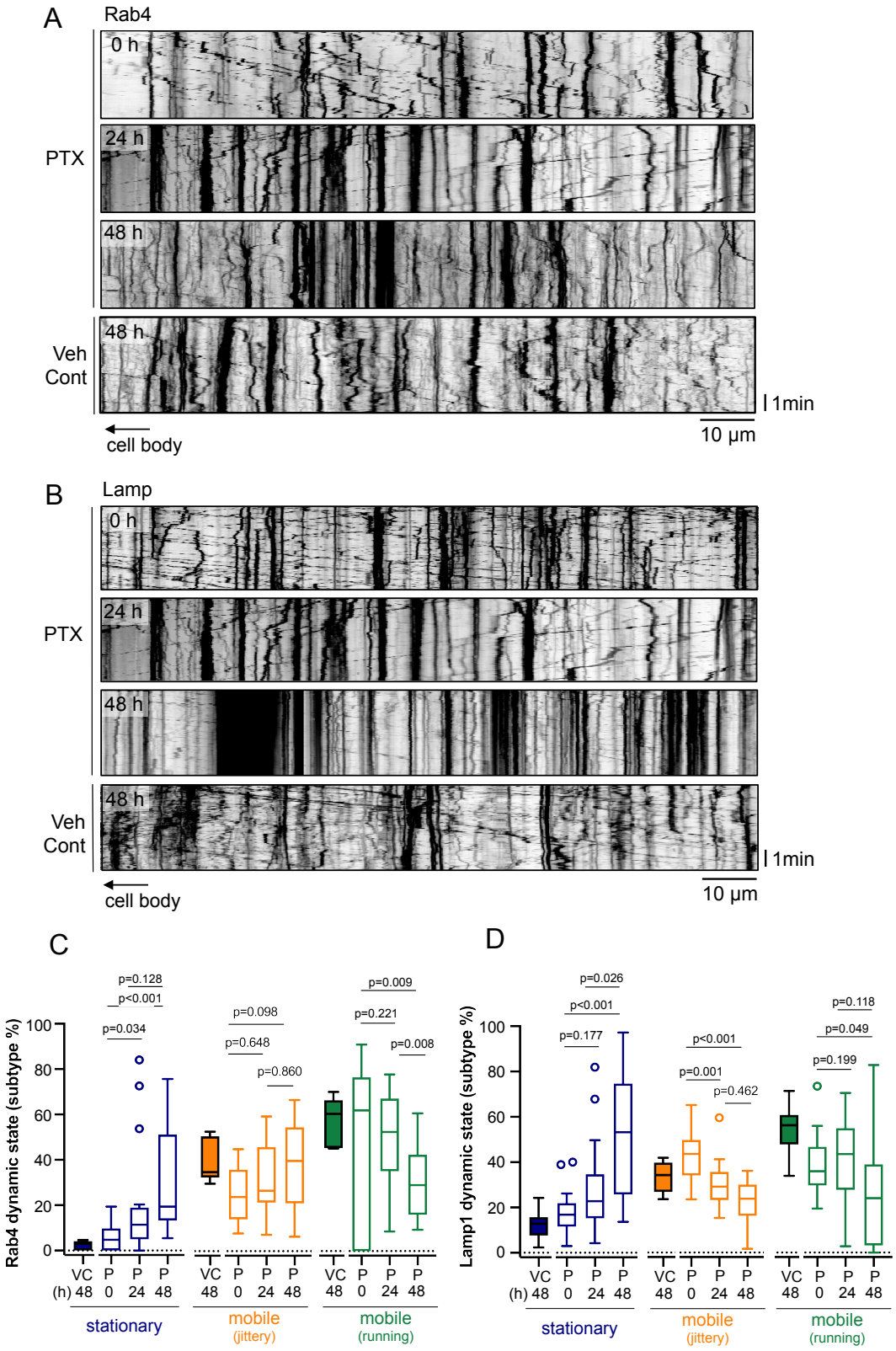

Fig. S11. Rab4 and Lamp1 positive vesicle motility is altered prior to degeneration of mouse DRG neurons *in vitro*

(*A* and *B*) Kymographs showing Rab4 positive (*A*) and Lamp1 positive (*B*) vesicle motility. Either mTagRFP-T-Rab4a-7 (Rab4) or Lamp1-mRFP-FLAG (Lamp1) was transduced in a dissociated adult DRG culture at DIV 3 reared in MatTek dish. The culture was treated with paclitaxel (50nM) starting at DIV 12, for 0, 24, or 48 h prior to imaging. Kymographs from DMSO (vehicle control) treated cells are shown as a control.

(*C* and *D*) Quantification of dynamic states of Rab4 positive and Lamp1 positive vesicles. Vesicles were categorized as either stationary or mobile. Mobile vesicles were further characterized as either jittery (movement < 5 pixels) or running (movement ≥ 5 pixels). VC denotes a vehicle control at 48 h and P denotes paclitaxel at 50 nM at 0, 24, and 48 h. VC is shown for a qualitative comparison. Data was collected from two independent experiments. All paclitaxel treated groups were subjected to Kruskal-Wallis test followed by Dunn's multiple comparisons test or Kolmogorov-Smirnov test. Error bars = S.D. See also Table S1 for further statistical description.

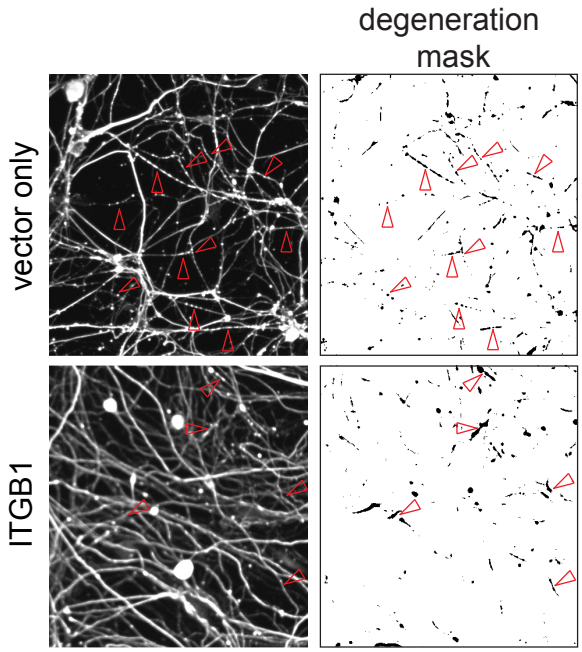

Fig. S12. Examples of degeneration mask for calculating degeneration index

Degeneration masks were generated according to Gerdts et al., 2011 (14). Arrowheads point to several examples of degenerating axons in the micrograph also seen in matching locations within degeneration masks.

Table S2. List of genotypes used in this study

Fig. 1	*w-; ppk1.9Gal4/+; ppkcd4tdgfp/+*	Crossed with w^{1118}
Fig. 2 *A, C, C′, E, F*	*w-; ppk1.9Gal4/+; ppkcd4tdgfp/+*	Crossed with w^{1118}
Fig. 2 *B, D, D′, E, F*	*w-; ppk1.9Gal4/+; ppkcd4tdgfp/ UASαPS1, UASβPS*	
Fig. 3 *A*	w^{1118} isogenized	
Fig. 3 *B*	*w-; ppk1.9Gal4/+; ppkcd4tdgfp/+* *w-; ppk1.9Gal4/+; ppkcd4tdgfp/ UASαPS1, UASβPS*	Crossed with w^{1118}
Fig. 4 *A, A′, C, C′, E–H*	*w-; ppk1.9Gal4/UAS Rab4-mRFP; ppkcd4tdgfp/+*	*UAS Rab4-mRFP* is originated from BL8505
Fig. 4 *B, B′, D, D′, I*	*w-; ppk1.9Gal4/+; ppkcd4tdgfp/UAS Spin-myc-mRFP*	*UAS Spin-myc-mRFP* is isolated from BL42716
Fig. 4 *J–P*	*w-; ppk1.9Gal4/UAS YFP-Rab4 WT; ppkcd4tdgfp/ UASαPS1, UASβPS*	*UAS YFP-Rab4 WT* is originated from BL23269
Fig. 5 *B–D*	*w-; ppk1.9Gal4/+; ppkcd4tdgfp/+* *w-; ppk1.9Gal4/UAS Rab4-mRFP; ppkcd4tdgfp/+*	Crossed with w^{1118}
Fig. 5 *E–G*	*w-; ppk1.9Gal4/UAS Rab4-mRFP; ppkcd4tdgfp/+*	
Fig. 6	Wildtype C57Bl/6J mice	
Fig. S1	*w-; ppk1.9Gal4/+; ppkcd4tdgfp/+*	Crossed with w^{1118}
Fig. S2	*w-; ppk1.9Gal4/+; ppkcd4tdgfp/+*	Crossed with w^{1118}
Fig. S3 *A–B’*	*w-; ppk1.9Gal4/ UAS-Ncad$^{7b\text{-}13a\text{-}18b}$; ppkcd4tdgfp/+*	
Fig. S3 *C* and *D*	*w-; ppk1.9Gal4/+; ppkcd4tdgfp/+* *w-; ppk1.9Gal4/+; ppkcd4tdgfp/ UASαPS1, UASβPS* *w-; ppk1.9Gal4/ UAS-Ncad$^{7b\text{-}13a\text{-}18b}$; ppkcd4tdgfp/+*	Crossed with w^{1118}

Fig. S4	*w-; UAS TrpA1/+; 412Gal4/+*	*UAS TrpA1* is isolated from BL26263
Fig. S5	*w-; ppk1.9Gal4/+; ppkcd4tdgfp/+* *w-; ppk1.9Gal4/UAS βPS RNAi; ppkcd4tdgfp/+* *w-; ppk1.9Gal4/+; ppkcd4tdgfp/ UASαPS1, UASβPS* *w-; ppk1.9Gal4/ UAS-Ncad$^{7b\text{-}13a\text{-}18b}$; ppkcd4tdgfp/+*	Crossed with *w^{1118}*
Fig. S6	*w-; ppk1.9Gal4/+; ppkcd4tdgfp/+* *w-; ppk1.9Gal4/UAS Rab4-mRFP; ppkcd4tdgfp/+*	Crossed with *w^{1118}*
Fig. S7	*w-; ppk1.9Gal4/UAS Rab4-mRFP; ppkcd4tdgfp/+*	
Fig. S8	*w-; ppk1.9Gal4/+; ppkcd4tdgfp/UAS Spin-myc-mRFP*	
Fig. S9 *A–C*	*w-; ppk1.9Gal4/UAS Rab4-mRFP; ppkcd4tdgfp/ UASαPS1, UASβPS*	
Fig. S9 *D–F*	*w-; ppk1.9Gal4/+; ppkcd4tdgfp/UAS Spin-myc-mRFP* *w-; ppk1.9Gal4/ ppkcd4tdgfp; UAS Spin-myc-mRFP/ UASαPS1, UASβPS*	
Fig. S10-12	Wildtype C57Bl/6J mice	

SI References

1. A. Burgos *et al.*, Nociceptive interneurons control modular motor pathways to promote escape behavior in Drosophila. *Elife* **7** (2018).

2. J. A. Ainsley *et al.*, Enhanced locomotion caused by loss of the Drosophila DEG/ENaC protein Pickpocket1. *Curr Biol* **13**, 1557-1563 (2003).

3. C. Han, L. Y. Jan, Y. N. Jan, Enhancer-driven membrane markers for analysis of nonautonomous mechanisms reveal neuron-glia interactions in Drosophila. *Proc Natl Acad Sci U S A* **108**, 9673-9678 (2011).

4. D. M. Gohl *et al.*, A versatile in vivo system for directed dissection of gene expression patterns. *Nat Methods* **8**, 231-237 (2011).

5. C. Huet-Calderwood *et al.*, Novel ecto-tagged integrins reveal their trafficking in live cells. *Nat Commun* **8**, 570 (2017).

6. J. Y. Jeong *et al.*, One-step sequence- and ligation-independent cloning as a rapid and versatile cloning method for functional genomics studies. *Appl Environ Microbiol* **78**, 5440-5443 (2012).

7. E. L. Gornstein, T. L. Schwarz, Neurotoxic mechanisms of paclitaxel are local to the distal axon and independent of transport defects. *Exp Neurol* **288**, 153-166 (2017).

8. J. Liu, S. Pasini, M. L. Shelanski, L. A. Greene, Activating transcription factor 4 (ATF4) modulates post-synaptic development and dendritic spine morphology. *Front Cell Neurosci* **8**, 177 (2014).

9. K. R. Smith *et al.*, Identification and characterisation of a Maf1/Macoco protein complex that interacts with GABAA receptors in neurons. *Mol Cell Neurosci* **44**, 330-341 (2010).

10. K. R. Smith *et al.*, GIT1 and betaPIX are essential for GABA(A) receptor synaptic stability and inhibitory neurotransmission. *Cell Rep* **9**, 298-310 (2014).

11. B. J. Matthews *et al.*, Dendrite self-avoidance is controlled by Dscam. *Cell* **129**, 593-604 (2007).

12. J. Schindelin *et al.*, Fiji: an open-source platform for biological-image analysis. *Nat Methods* **9**, 676-682 (2012).

13. S. Q. Liu, D. H. Zhang, Y. Song, H. C. Peng, W. D. Cai, Automated 3-D Neuron Tracing With Precise Branch Erasing and Confidence Controlled Back Tracking. *Ieee T Med Imaging* **37**, 2441-2452 (2018).

14. J. Gerdts, Y. Sasaki, B. Vohra, J. Marasa, J. Milbrandt, Image-based Screening Identifies Novel Roles for I kappa B Kinase and Glycogen Synthase Kinase 3 in Axonal Degeneration. *J Biol Chem* **286**, 28011-28018 (2011).

15. L. Chen *et al.*, Mitochondria and Caspases Tune Nmnat-Mediated Stabilization to Promote Axon Regeneration. *PLoS Genet* **12**, e1006503 (2016).

16. S. Neumann, R. Chassefeyre, G. E. Campbell, S. E. Encalada, KymoAnalyzer: a software tool for the quantitative analysis of intracellular transport in neurons. *Traffic* **18**, 71-88 (2017).

17. A. G. York *et al.*, Instant super-resolution imaging in live cells and embryos via analog image processing. *Nat Methods* **10**, 1122-1126 (2013).

18. S. Berg *et al.*, ilastik: interactive machine learning for (bio)image analysis. *Nat Methods* **16**, 1226-1232 (2019).

19. T. A. Ferreira *et al.*, Neuronal morphometry directly from bitmap images. *Nat Methods* **11**, 982-984 (2014).